SAE INTERNATIONAL

ARTICLE INFO
Article ID: 03-18-01-0003

doi:10.4271/03-18-01-0003

Additively Manufactured Lightweight Automobile Cylinder Head—A New Process for Structural Optimization from Concept to Validated Hardware

Can Kayacan,[1] Stefan Pischinger,[1] Klaus Ahlborn,[2] and Jan Bültmann[3]

[1]TME | RWTH Aachen University, Germany
[2]DEUTZ AG, Germany
[3]INPECA GmbH | BÖLLINGER GROUP, Germany

Abstract

Reducing vehicle weight is a key task for automotive engineers to meet future emission, fuel consumption, and performance requirements. Weight reduction of cylinder head and crankcase can make a decisive contribution to achieving these objectives, as they are among the heaviest components of a passenger car powertrain.

Modern passenger car cylinder heads and crankcases have greatly been optimized in terms of cost and weight in all-aluminum design using the latest conventional production techniques. However, it is becoming apparent that further significant weight reduction cannot be expected, as processes such as casting have reached their limits for further lightweighting due to manufacturing restrictions. Here, recent developments in the additive manufacturing (AM) of metallic structures is offering a new degree of freedom.

As part of the government-funded research project LeiMot [Lightweight Engine (Eng.)] borderline lightweight design potential of a passenger car cylinder head with the use of automated structural optimization is investigated. A four-cylinder 2.0 L series production Diesel engine cylinder head is taken as basis in terms of bolting and gas flow channels.

With the newly gained design freedom by AM, it is demonstrated that a cylinder head with up to 30% weight reduction in comparison to the reference cylinder head can be realized through a novel stiffness concept, while fulfilling the mechanical requirements. The optimized design is initially validated by CAE methods for the hot operational conditions and worst-case circumstances. Required material properties are determined through manufactured specimens. A prototype cylinder head is manufactured using the LPBF (laser powder bed fusion) process, and hardware durability is validated on a hydro-pulse test bench under the maximum cylinder pressure of the reference Diesel engine. Subsequently, a material analysis is performed, and optimization potentials at the component geometry and printing parameters are investigated to further improve material properties and hence fatigue performance.

History

Received: 15 May 2024
Revised: 10 Jul 2024
Accepted: 06 Sep 2024
e-Available: 25 Sep 2024

Keywords

Additive manufacturing, Lightweight, Laser powder bed fusion, Cylinder head, Topology optimization, Bionic design, Powertrain

Citation

Kayacan, C., Pischinger, S., Ahlborn, K., and Bültmann, J., "Additively Manufactured Lightweight Automobile Cylinder Head—A New Process for Structural Optimization from Concept to Validated Hardware," *SAE Int. J. Engines* 18(1):19-37, 2025, doi:10.4271/03-18-01-0003.

ISSN: 1946-3936
e-ISSN: 1946-3944

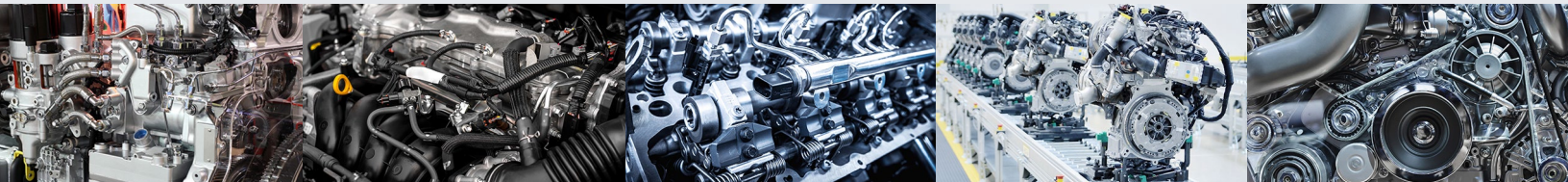

Introduction

Weight reduction has been one of the most important goals of vehicle design due to its environmental impact, costs, vehicle dynamics as well as customer satisfaction. There is continuous research on new design approaches, alternative materials, and manufacturing processes to achieve further lightweighting [1, 2, 3, 4].

From the establishment of the first-ever automobile emission control regulations in 1966 to the first Euro emission standards in 1991 [5], the transport industry is under continuously tightened obligation to produce vehicles with less fuel consumption and exhaust gas emissions in all major markets [6, 7, 8], as a main contributor of global emissions [9]. Figure 1 shows the potential impact of 100 kg weight reduction on CO_2 emission and fuel consumption reductions in a WLTP cycle. For gasoline and Diesel engines, secondary savings are considered (constant power-to-weight ratio) in addition [10]. Including primary and secondary savings, a 100 kg weight reduction results in approx. 0.24 L/100 km less fuel consumption for a Diesel powertrain in the low part of the WLTP cycle (with speeds below 60 km/h) and 8 g/km CO_2 reduction. Primary savings are considered direct savings due to weight reduction without any other vehicle adjustments. Further adjustments such as engine downsizing or optimization of torque curves are considered secondary savings. In addition to the impact of reduced energy requirement through lightweighting, the reduced material volume also has a direct contribution to emission reduction during the engine cold start phase, where the highest portion of total emissions occur [11]. During transient heat transfer, components reach their operational temperatures faster due to reduced thermal inertia, increasing the warm-up rate of lubricant and coolant [12]. In addition to the positive impacts of lightweighting on the environment and costs, it also contributes to driving performance and hence to customer satisfaction with improved maneuverability, acceleration, and braking.

Powertrain weight accounts for approx. 25% of the total weight of a passenger car [13] and 16% of the total weight of a light-duty commercial vehicle [14]. Finding solutions to reduce the mass of the heaviest components of a powertrain, such as cylinder head and crankcase, can make a decisive contribution to meet the above-mentioned objectives. Under continuously increasing performance demands, e.g., due to downsizing concepts [15], cylinder head, and crankcase in all-aluminum design have been continuously optimized in terms of cost and weight using the latest conventional production techniques. However, it is becoming apparent that further significant weight reduction while satisfying durability requirements cannot be expected with conventional techniques, which is shown in Figure 2. As processes such as casting have reached their limits due to manufacturing restrictions, recent developments in additive manufacturing (AM) are offering new possibilities for further weight reduction. Significantly fewer manufacturing restrictions of AM allow bionic design

FIGURE 1 Effect of 100 kg vehicle mass reduction on CO_2 emission and fuel consumption reductions for constant power-to-weight ratio.

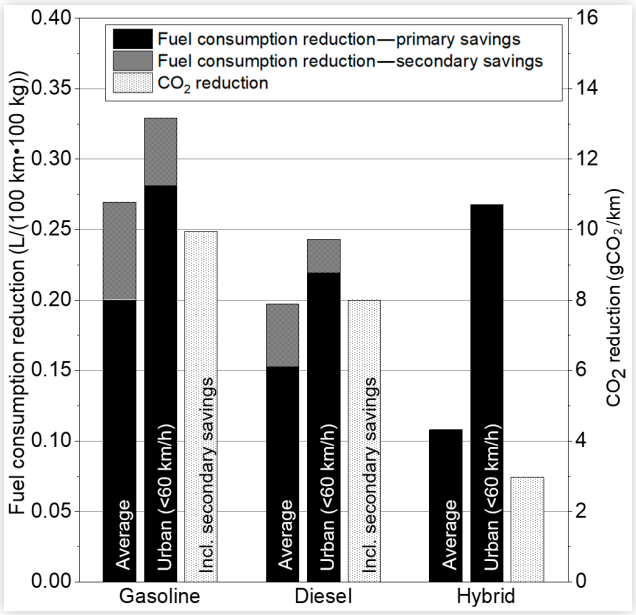

FIGURE 2 Development of weight-to-power ratio of series engines over time.

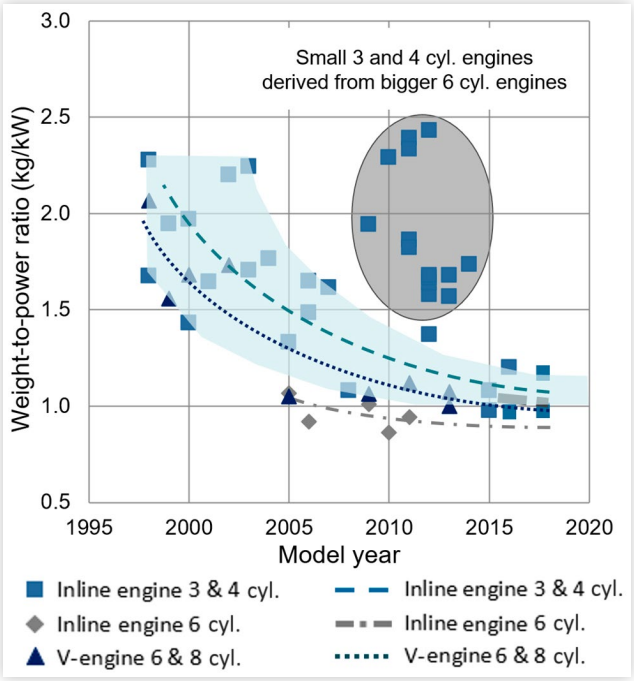

tailored to load paths within the structure with thinner and nonuniform wall thicknesses, holes with smaller diameters, and compact design. Nevertheless, the maximum size of producible components is restricted by machine size. In addition, closed volumes should be designed suitably for ease of depowdering and to avoid eventual limitations in function due to the formation of support structures [16, 17].

In case of lightweight design for AM, following a conventional parametric component design approach for the purpose of maximum weight reduction prevents taking full advantage of the design degree of freedom brought by AM. Since the definition of optimization potential is conventionally highly dependent on engineering judgment without exact knowledge of structural load patterns, integrating automated topology optimization as an effective computer-aided engineering (CAE) method [18] into the concept design phase may help achieve a borderline lightweight concept. In this work, a new cylinder head design process based on automated topology optimization (TO) is proposed with the target of achieving a borderline lightweight passenger car cylinder head for AM.

According to extensive literature research, no similar application of TO is known to the authors of this work until now. On the other hand, within other powertrain components, pistons have been widely analyzed in terms of its weight reduction potential using TO for AM [19]. In fact, a topology-optimized and additively manufactured lightweight piston is already being used in a small series high-performance engine, enabling a significant increase in the rated power of the engine [20]. Brackets [21, 22], subframes [23], and chassis [24, 25, 26] are among other vehicle parts, which have been investigated for the application of automated TO.

It has been demonstrated that with use of TO further weight reduction can be achieved in comparison to a manually optimized cylinder head, where series development criteria in terms of function and durability are fully met. The durability of the cylinder head has been initially validated by CAE with worst-case boundary conditions. After CAE validation, a prototype cylinder head was manufactured with LPBF (laser powder bed fusion) process using AlSi10Mg alloy, and fatigue durability of the hardware was validated with a hydro-pulse test under the maximum cylinder pressure of the reference cylinder head. Subsequently, cylinder pressure has been further increased in order to analyze the fatigue limit of the cylinder head and validate the CAE simulation approach. The fracture mechanism and the microstructure of the AM material have been analyzed and further optimization potentials for improved component durability have been discussed.

As reference the cylinder head of a four-cylinder, 2.0 L, 120 kW series production Diesel engine has been obtained with a weight-to-power ratio of 1.2. Global properties such as bore, cylinder distance, gas flow channels, and mounting parts have been kept unchanged. A highly efficient cooling concept (arterial cooling) has been adopted from another lightweight cylinder head prototype, which is developed in the scope of the LeiMot research project for AM and introduced in previous publications [27, 28, 29].

Automated Topology Optimization

In general terms, structural optimization is defined as realizing the best possible structural design with a defined objective and some limitations [30]. To develop a novel stiffness concept, this study investigates the application of TO, which is the most general form of structural optimization as a material distribution problem. Hence, other types of structural optimization, shape, and size optimizations [31] are not considered in the scope of this work.

For the automated TO, Altair Optistruct 2021 has been used, which is one of the major software packages used in the commercial market for structural optimization [32]. Optimization has been performed with the SIMP (solid isotropic material with penalization) method [33] as the most used method for TO in the commercial field [34]. The optimization problem is defined as finding the optimal material distribution, which minimizes the compliance (optimization objective), in other words, maximizes the stiffness, while being subjected to an upper volume boundary (optimization constraint). The general optimization problem can be formulized as follows [35]:

$$\text{Find: } \rho = \left\{\rho_1, \rho_2, \ldots, \rho_N\right\}$$

$$\text{Minimize: } C = \mathbf{f}_p^T \mathbf{u}_p$$

Subjected to:

$$\sum_{e=1}^{N} \rho_e v_e \leq V^*$$

$$0 < \rho_{\min} \leq \rho_e \leq 1$$

ρ indicates the vector of design variables, whereas an FE model with an N total number of FE, each element owns an artificial density. After every optimization iteration, each element density can obtain a value between 0 (void) and 1 (full material). Compliance C, which is the inverse of stiffness, is defined as the virtual work of the loads on the displacements of application points [36] and calculated by the multiplication of the external force **f** and the displacement **u** vectors for the nodal degree of freedom p. Since the displacement vector is dependent on the global stiffness matrix, at the SIMP method Young's

modulus of each FE is calculated as a function of the artificial element density ρ according to equation [35]:

$$E_e = \rho_e^n E_0$$

where E_0 indicates the Young's modulus of the bulk material and n is the penalization factor, which penalizes the intermediate densities to 0 and 1 to achieve a discrete optimization result [37]. Finally, according to the defined optimization constraint sum of the individual artificial volume of each FE ($\rho_e v_e$) should be equal to or lower than the given volume as the optimization constraint. The result of the optimization with the described objective and constraint functions (minimum compliance and volume constraint) has been compared with other possible alternative problem definitions and regarded as the most suitable problem definition for this application.

The optimization process is shown in Figure 3. Initially, a finite element analysis (FEA) is performed and subsequently, convergence of the results is checked for the defined optimization problem. If convergence criteria are not fulfilled, a sensitivity analysis is performed to determine the sensitivity of structural responses with respect to design variables. For the efficiency of the calculation, approximate explicit models are built and design variables are updated for the next iteration [38].

FIGURE 3 Iteration process of SIMP.

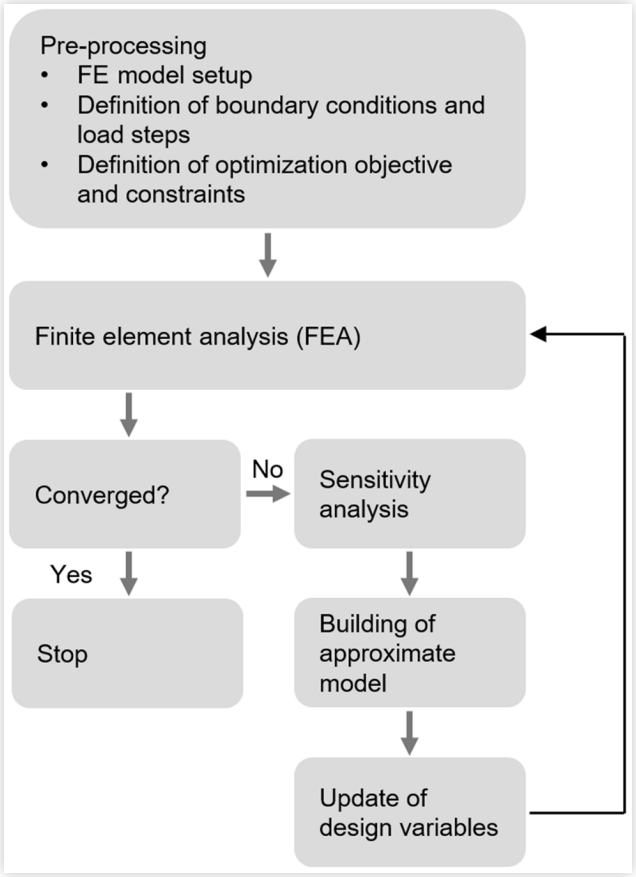

FE Model Setup

Usage of the reference cylinder head geometry for the optimization would lead to suboptimal results, since a novel and bionic stiffness concept using the full potential of the available package cannot be achieved but may only serve for the optimization of the structure within its existing geometrical boundaries. In order to provide the optimization algorithm with the highest possible design freedom and to obtain an optimal material distribution, the largest available package volume should be considered in the created FE model as "design space" of the TO.

Features that are necessary for the function of the cylinder head cannot be included in the discretized domain for the optimization (non-design space). Gas, coolant, and pressured oil channel surfaces, bolt boss as well as contact surfaces to the other components (injector, glow plug, valve seat and valve guide, valve spring, hydraulic valve adjuster (HLA), cylinder head gasket, camshaft ladder frame, intake and exhaust manifolds) have been considered in the optimization model as a separate solid FE component with 3 mm wall thickness, which is the defined minimum wall thickness for the cylinder head. Modeling of the non-design space as a solid 3D structure is advantageous over modeling with 2D FE surfaces due to more realistic stiffness distribution in the global model and for the ease of the subsequent design step. Oil return channels haven't been considered in the optimization model in order to use the topological features of the optimization result for the guidance of the oil. Figure 4 shows the FE model for the TO with the design and non-design spaces, having a total of ~12 million first-order FE elements and ~2.5 million nodes. Cylinder head design/non-design spaces and dummy crankcase have been discretized with linear tetrahedrons, whereas cylinder

FIGURE 4 FE model of the cylinder head and dummy crankcase compound in exploded view.

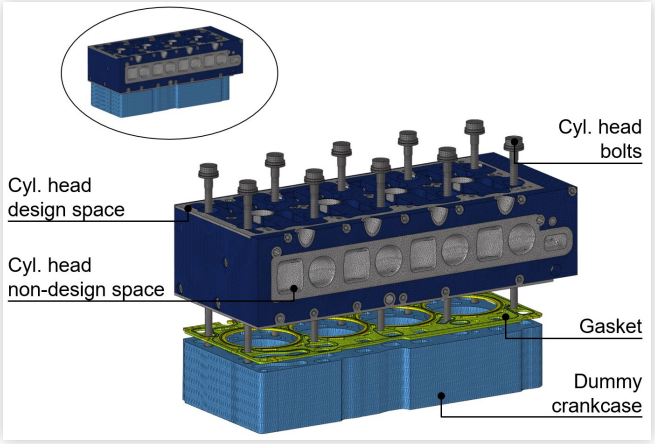

head bolts including washers and gaskets are discretized with linear hexahedrons. A parameter study on the 3D discretization parameters showed that in order to obtain a smooth and bionic surface contour, element growth shouldn't be allowed during the automated 3D discretization. The usage of established 3D FE discretization parameters of a typical stress analysis will lead to bad topological contour in the optimization results, where bigger 3D element sizes are allowed at the areas far away from the surface to reduce the computational times in a stress analysis.

Load Case Definition

Load steps in a typical FE analysis for high-cycle fatigue (HCF) evaluation are defined according to the real load sequence during engine operation, where initially assembly loads are applied at cold conditions with subsequent thermal expansion of the structure and cylinder pressure loads according to the given firing order of the engine. Since for the fatigue analysis mean and amplitude stresses are calculated from cyclic loads, consideration of above-mentioned loads in discrete load cases is necessary.

Since the task of TO is different than a HCF analysis, it is possible to reduce the simulation time significantly by considering all mechanical load cases in a single load case for the FEA during the optimization iterations. In order to validate the approach with simplified load case definition, for each load source individual analyses have been performed and strain energy distributions within the structure have been compared with the combined load case.

At rated power, the combustion chamber heat load causes thermal expansion of the aluminum material with structural temperatures up to 260°C. Consideration of thermal expansion for the compliance calculation tends to reduce material volume. As thermal load dominance increases in the system in comparison to mechanical loads, this behavior may result in topologies with lower strength [39]. As thermal loads do not influence the main load patterns of the cylinder head, during the TO of this work only mechanical loads are considered. Nevertheless, thermal expansion can be considered as a separate load step during the FE analysis prior to the mechanical load step in order to constrain structural deformations at critical areas. As an example, constraining the valve guide misalignment relative to the valve seat rings can result in stiffening of the corresponding area and hence less wear at the valve edges during the operation of the engine. According to the optimization definition, the optimization algorithm alters artificial element densities to meet the defined volume target with the highest possible overall structural stiffness. This results in the highest load source dominating the optimization result, in this case, cylinder head bolt pretension. In an extreme case, no proper connection of structures with the main body will occur, e.g., for the bolt bosses at the outer periphery of the cylinder head. In order to realize the structural connection of all load-carrying functional surfaces, a sensitivity study has been performed in which applied loads are artificially adjusted. Figure 5 shows the considered mechanical loads for the TO.

During the LPBF process support structures are used to allow thermal dissipation, printability, and part

FIGURE 5 Applied mechanical loads in the topology optimization.

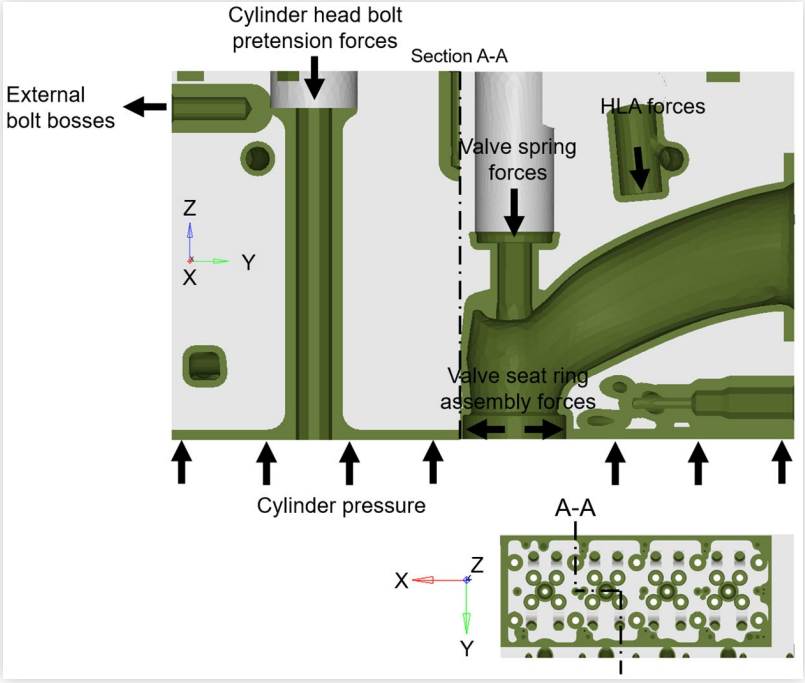

balance [40]. An objective of design for AM (DfAM) is minimizing the necessity for support structures by adapting the component topology, which saves material and reduces production and post-processing times [41]. For this purpose, an overhang constraint has been defined according to the predefined build direction of the cylinder head on the build plate. Other considered optimization parameters include minimum dimension (MINDIM) to avoid the formation of walls with small thicknesses, checkerboard control to avoid discrete solutions between neighboring FE [42], and penalty factor to penalize the artificial element densities.

TO Simulation

TO performed with 98 CPUs and 2 MPI processes on two nodes in "in-core" mode has a runtime of ~25 h. A minimum compliance objective with linear–static FEA has been achieved after 18 iterations.

As can be seen in Figure 6, purposed design topology shows an overall bionic architecture without sharp edges, where the load transfer is realized from the shortest path possible. Results show that the material is mainly gathered around the cylinder head bolt bosses, serving as a pivot structure for the structural integrity. Large cavities are formed between the cylinders, which are opening to the outside of the cylinder head. Non-design materials, which are located on the load transfer paths have been connected with the optimized design domain and used for the global stiffness. At the outer periphery all bolt bosses are connected with the main structure and HLA housings are supported in a vertical direction above the gas exchange ports. A density threshold of 0.7 has been selected for the export of the optimization results for final geometry creation in CAD.

Final Design with CAD

Based on the TO result the final geometry of the cylinder head has been modeled in CAD. In order to validate the reliability of the optimization method, it is pursued to generate the final geometry without any deviation from the optimization results. Important features, which are additionally considered during the design of the final model, include:

- Radii between the design and non-design domains
- Oil sealing wall with 2 mm thickness above the gas channels. A honeycomb pattern is implemented to reduce the negative effect of thin walls on NVH performance
- Oil return channels for the transfer of oil to the crankcase oil return channels using the existing material for channel boundaries

The developed oil return concept takes advantage of the existing cavities in the topology without impairing the cylinder heads' stiffness concept. Collected oil over the bottom plate of the cylinder head is transferred to the oil return channels of the crankcase at both the intake and exhaust sides of the cylinder head.

Figure 7 shows the final CAD model of the cylinder head as the raw part to be used for the LPBF process, where thread holes, as well as flange surfaces for other components, are considered with sufficient material for the machining process.

After creating the final machined model in CAD, a 30% weight reduction over the cylinder head of the reference engine is achieved. Consideration of additional geometrical features such as sealing wall and connection

FIGURE 6 Result of the automated topology optimization with design (light gray, density threshold 0.7) and non-design (dark green) domains; isometric view (left) and cross-sectional views (right).

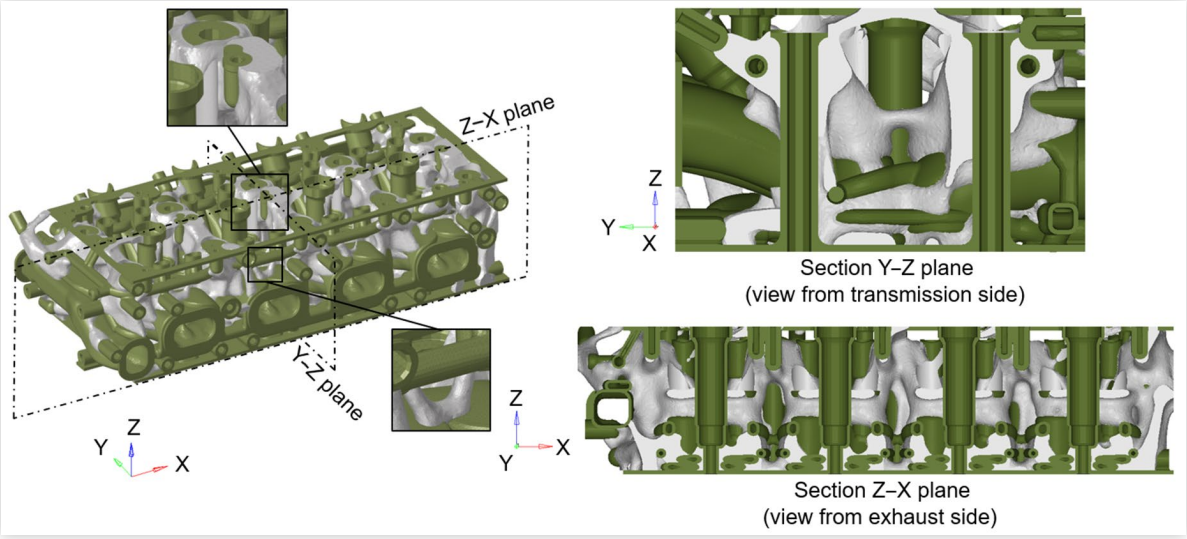

FIGURE 7 Final CAD model of the cylinder head as raw part for LPBF process.

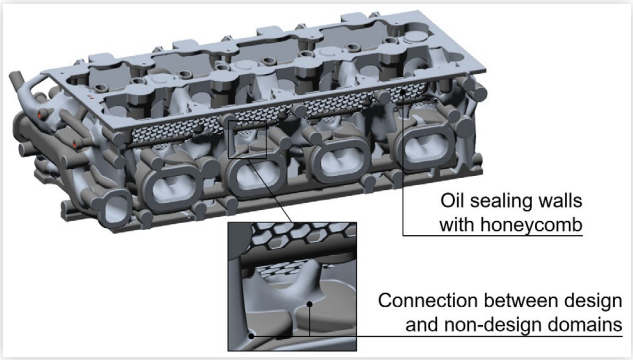

radii between the design and non-design domains increased the overall weight only by −400 g (Figure 8).

FIGURE 9 FE model for the HCF analysis of the cylinder head (cylinder head shown as transparent).

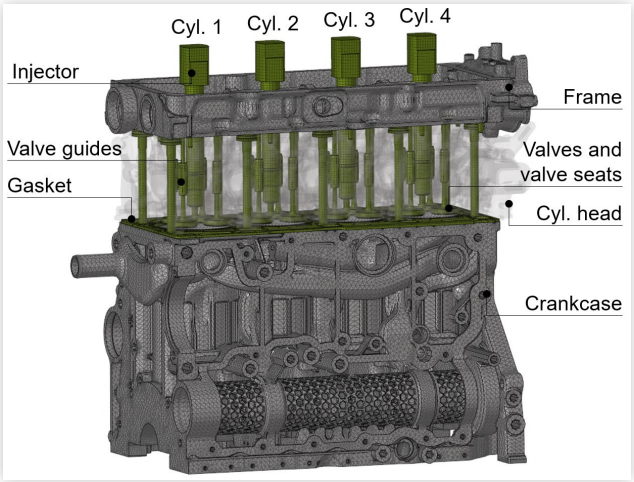

Validation of Durability with CAE

HCF Analysis

HCF performance of the cylinder head has been analyzed with Abaqus 2017 and FEMFAT 6.14 according to the worst-case series development criteria for the rated power operation point of the reference engine (120 kW at 3250 1/min, lower boundary of the rated speed range due to worse cooling-performance). Discretized FE model of the cylinder head and crankcase compound including the relevant parts for the analysis have been shown in Figure 9. Initially, a thermal analysis has been performed in order to obtain the nodal temperatures to be considered in the thermomechanical analysis. Heat transfer coefficient (HTC) distribution of the coolant as well as HTC and temperature distribution of the combustion gas at the areas close to the structure surfaces have been obtained from 3D CFD analyses and mapped to the FE model as boundary conditions for the thermal analysis [43]. Subsequently, a quasi-static nonlinear thermomechanical analysis has been performed with linear elastic material properties. For each simulated load step material stresses are obtained to be used in the subsequent durability analysis for the evaluation of fatigue safety factors for 90% component survival rate based on the cyclic mean and amplitude stresses.

Additionally, contact pressures have been analyzed in a separate analysis, e.g., to evaluate the sealing performance of the cylinder head gasket.

Thermomechanical analysis for HCF evaluation has been performed according to the below load case (LC) sequence:

- LC1 (cold assembly): Application of maximum bolt forces to the cylinder head, ladder frame, and injector, maximum press fits of the valve seats and valve guides
- LC2 (thermal load): Thermal expansion of the structure according to the mapped nodal temperatures
- LC3: 150 bar max. cyl. pressure at cyl. 1
- LC4: 150 bar max. cyl. pressure at cyl. 3
- LC5: 150 bar max. cyl. pressure at cyl. 4
- LC6: 150 bar max. cyl. pressure at cyl. 2
- LC7: Relaxation to warm assembly

In order to consider the worst-case contact situation during cold engine start, a contact evaluation has been performed without the application of thermal load according to the following LC sequence:

FIGURE 8 Final cylinder head mass comparison with the reference cylinder head.

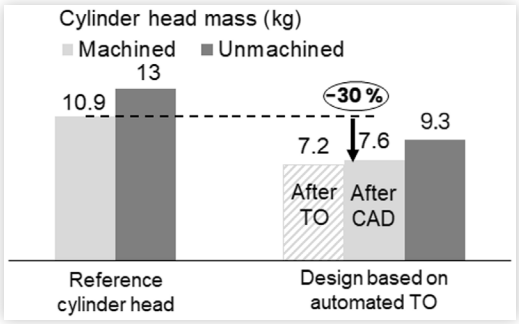

- LC1 (cold assembly): Application of min. bolt forces to the cylinder head, ladder frame, and injector bolt forces, minimum Press fits of the valve seats and valve guides
- LC2: 150 bar max. cyl. pressure at cyl. 1
- LC3: 150 bar max. cyl. pressure at cyl. 3
- LC4: 150 bar max. cyl. pressure at cyl. 4
- LC5: 150 bar max. cyl. pressure at cyl. 2
- LC6: Relaxation to cold assembly

AlSi10Mg LPBF Material Properties

Consideration of correct material properties in CAE is necessary for validating component durability. Material properties of casted components in AlSi10Mg are well-known nowadays and show statistically small scattering with well-established heat treatment parameters. Compared to cast material, components produced by LPBF show a unique and fine microstructure in as-built condition, where in contrast to cast material quasi-static strength values, tensile and yield strength are the highest, however with low ductility. In order to increase the elongation at break a subsequent heat treatment process is necessary.

Test samples have been manufactured in different build directions to determine the material properties for the CAE analysis and a quasi-static tensile test has been performed at room as well as at elevated temperatures. A T6 heat treatment is applied with two different artificial aging durations for the comparison of its effect on final mechanical properties:

- HT1: Solution annealing for 6 h at 515°C, water quenching at 80°C, and artificial aging for 12 h at 200°C
- HT2: Solution annealing for 6 h at 515°C, water quenching at 80°C, and artificial aging for 3 h at 200°C

Results show a typical temperature dependence, where the highest ultimate strength and Young's modulus are obtained at the 20°C room temperature, as can be seen in Figure 10. Values between different build directions show a larger scattering at higher temperatures. On the other hand, average values between different build directions are on a similar level, which supports the findings of other research work that material anisotropy is minimized after heat treatment [44, 45, 46]. Shortening the artificial aging duration to 3 h resulted in less scattering in the results and an increase in the average tensile strength and Youngs's modulus at 250°C. Hence, for the CAE analyses isotropic material properties have been defined using the worst material values from the tensile test samples with 3 h artificial

FIGURE 10 Ultimate strength and Young's modulus of the AlSi10Mg test samples manufactured with LPBF and heat treated with different artificial aging (AA) durations.

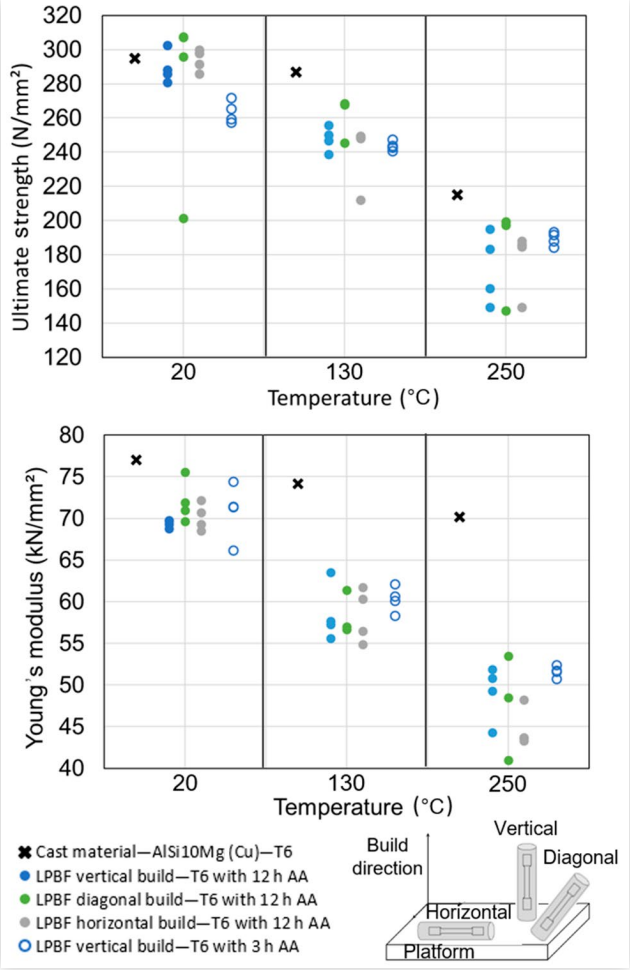

aging. In comparison to the reference cast material, LPBF samples showed significantly lower ultimate strength and Young's modulus values at the elevated temperatures of 130°C and 250°C. Despite the differences in manufacturing techniques and heat treatment parameters, the Cu content of the reference aluminum alloy significantly contributes to the deviation at elevated temperatures. On the other hand, higher material strength due to Cu content trades off with lower heat conductivity, which may lead to critical areas at the flame deck region due to high structural temperatures [47, 48].

The fatigue performance of LPBF AlSi10Mg is mainly defined by inherent defects within the material in the form of porosities, incomplete fusion holes, and cracks [49]. To determine the alternating strength of the LPBF material test samples have been manufactured and a fatigue test has been performed according to the staircase method ($R = -1$). Results are shown in a Wöhler diagram in Figure 11. Four samples showed no defect after 10^7 load cycles; however, a large scattering in their

FIGURE 11 Wöhler diagram for the fatigue test of AlSi10Mg samples manufactured with LPBF.

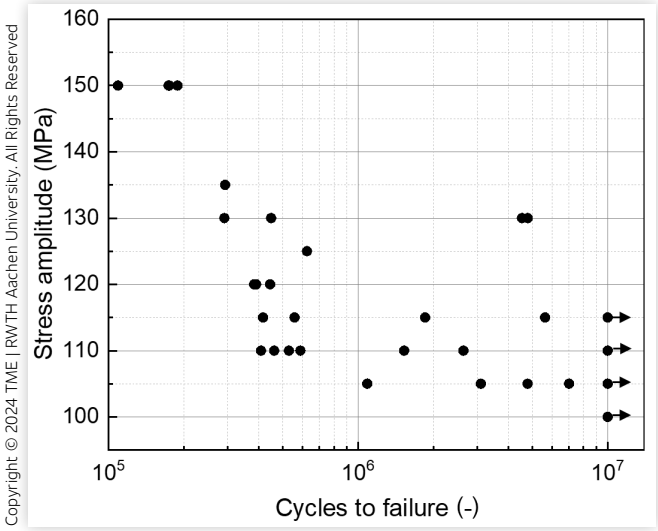

stress amplitudes is observed. In the CAE analysis, the worst-case material properties are considered by using a minimum measured alternating strength of 100 MPa from the four run-out samples.

Simulation Results

Thermal analysis results showed that similar surface temperature distributions prevail at each cylinder section, where the highest structural temperatures appear at the flame deck region of cylinder 1 with a maximum of 257°C, which is below the admissible maximum temperature of the material (Figure 12). On the other hand, the highest water jacket surface temperatures appear at a local region, closest to the combustion chamber surface, having a maximum value of 219°C. According to the additional boiling analysis no risk of film boiling is observed.

Thermomechanical durability has been evaluated by calculating fatigue safety factors at each FE node. In order to consider a probability of one defect per million parts, a minimum safety factor of 1.5 has been obtained for constant mean stress (σ_m = const.) and 1.25 for constant stress ratio (R = const.) as design criteria. Analysis showed that automated TO proposed an overall durable stiffness concept. The lowest fatigue safety factors are observed at the lower section of large cavities between the cylinders. These local areas are subjected to high mean stresses due to their locations directly above the stiff stopper bead section of the cylinder head gasket. Nevertheless, safety factors fall below the design criterion only at a local point, as shown for σ_m = const. in Figure 13, which is deemed as uncritical.

The minimum safety factor on the surface of the water jacket is 1.29 for R = const., located on a local area between the cylinders (Figure 14). It can be concluded

FIGURE 12 Temperature distribution on the flame deck surface of cylinder 1 (upper) and the water jacket surface (lower) at rated power.

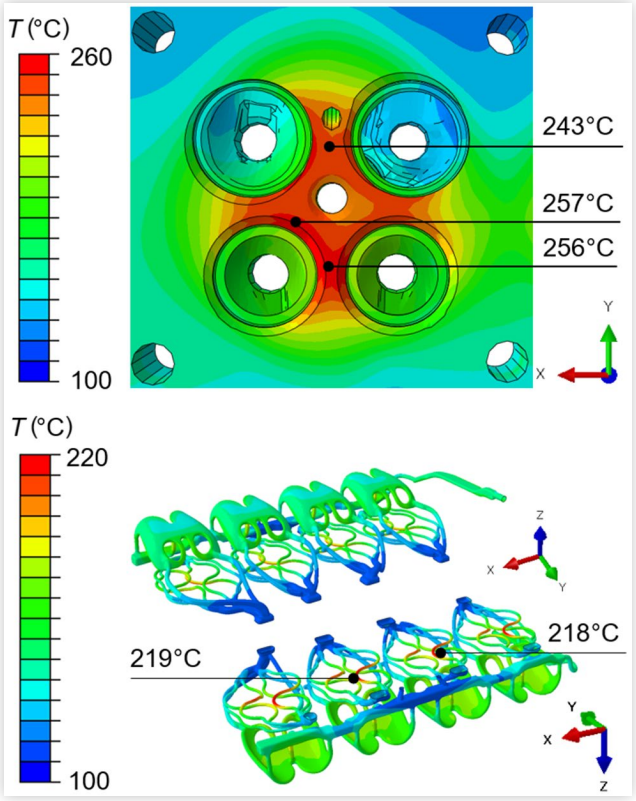

that the arterial cooling concept with small channel diameters (–3 mm) increased the overall stiffness at the flame deck area and provided TO with a larger design domain for optimal material distribution. In comparison, relatively large coolant channel volumes of a conventional cylinder head typically lead to high stresses and hence lower safety factors at the highly loaded flame deck area.

Only a few local areas of the cylinder head with high stress concentrations require optimization by radius adjustments, so that the fatigue safety of the overall cylinder head remains above the defined design criteria with sufficient margins.

The sealing performance of the cylinder head gasket has been validated under worst-case conditions by evaluating the contact pressures on the bead sections at cold conditions with minimum bolt pretension forces. Due to the higher thermal expansion of aluminum during engine operation the constraining steel bolts lead to an overall higher level of contact pressure on the combustion chamber beads compared to cold conditions. On the other hand, due to the thermal deformation of the component lower contact pressures are observed at the outer regions of the cylinder head in warm conditions, where water and oil beads are located. Nevertheless, minimum contact pressure values remain above the

FIGURE 13 Areas with relatively low safety factors on the bottom plate of the cylinder head.

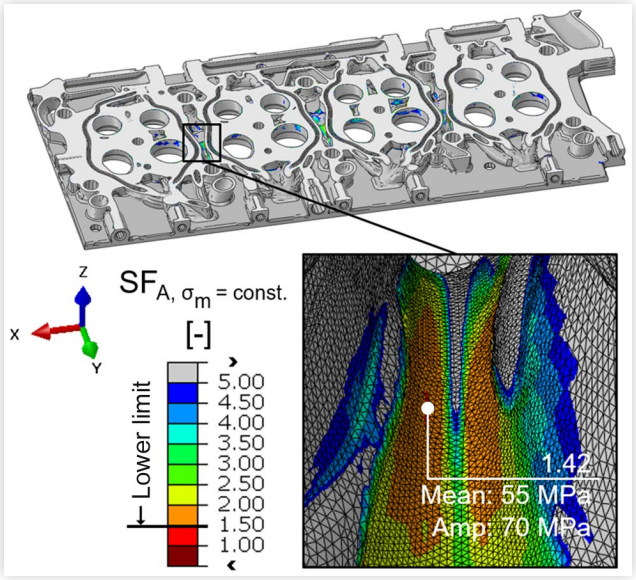

FIGURE 15 Minimum line pressure on water and pressurized oil beads of the cylinder head gasket.

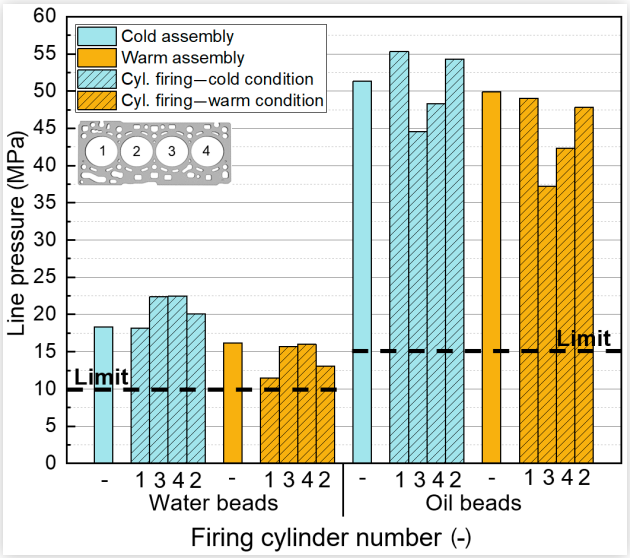

defined design target for both water and pressurized oil beads, as can be seen in Figure 15.

Minimum contact pressures on the combustion chamber beads of each cylinder are higher than the design criterion (5 × peak firing pressure of the engine) under operating conditions, as shown in Figure 16. Maximum overall gap movements of the full beads during the firing of the cylinders remain far below the design target (max. 20 μm), hence no fracture is expected.

CAD & CAE Workflow

In Figure 17, cylinder head development processes with CAD/CAE are compared for the conventional casting process and a lightweight cylinder head designed for AM. Higher interaction between CAD and CAE is required for the development process of an additively manufactured cylinder head, where CAE is not only used for validation and design optimization purposes but also as a major tool for defining the stiffness concept in the early concept stage. A design process driven by automated TO also requires incorporating manufacturing during the early concept stage for the consideration of process related restrictions according to DfAM (e.g., definition of build direction for the manufacturing of channels without support structures).

FIGURE 14 Lowest safety factor on the surface of the coolant channel.

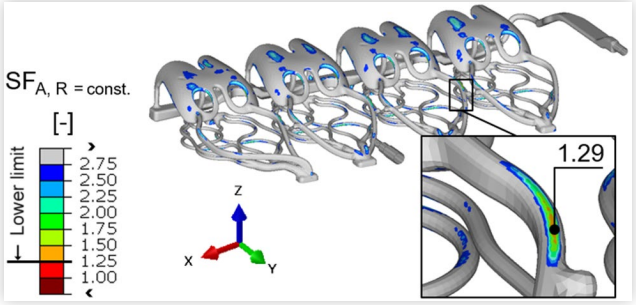

FIGURE 16 Minimum line pressure and maximum overall sealing gap movement of the combustion chamber beads.

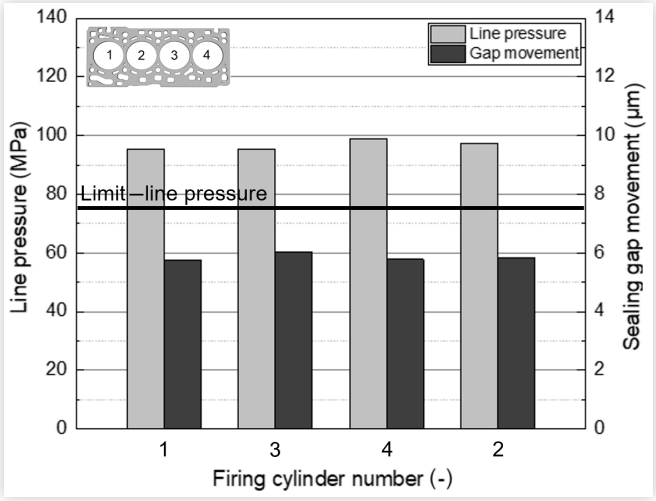

FIGURE 17 Comparison of cylinder head development processes with CAD/CAE: Conventional vs. to driven design approach for additive manufacturing.

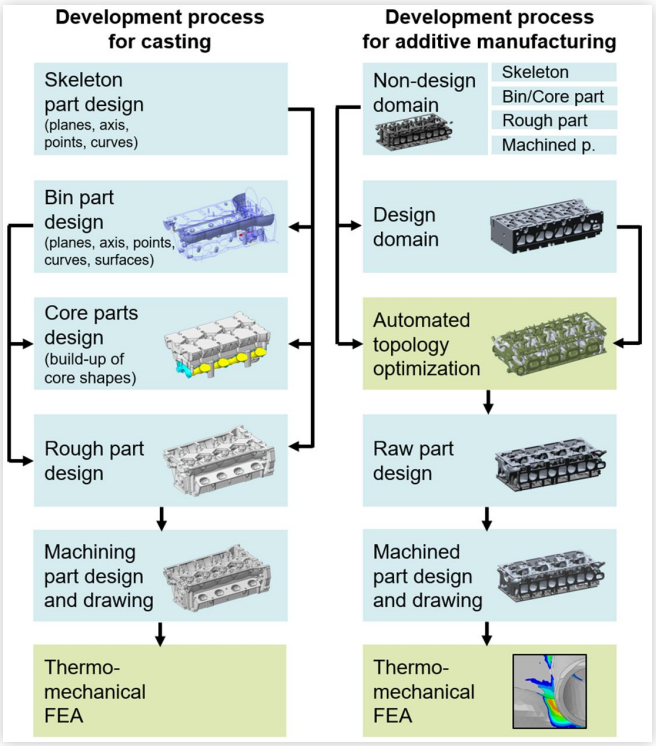

Manufacturing of the Prototype

The cylinder head was manufactured using the LPBF process. The machine used was an X Line 2000 R including the newest BCX upgrade, which features a build volume of 400 × 800 × 500 mm and two 1000 W lasers, one for each half of the build envelope. The lasers are operating in staggered order to ensure a clear and smoke-free optical trajectory for both lasers. Additionally, the process chamber features an optimized upper and lower gas flow. The upper gas flow is a high-volume gas flow to keep the chamber windows free of smoke and powder particles. The lower gas flow features a high flow uniformity and high velocity over the powder bed to remove the smoke and spatter quickly out of the process area.

The powder used for the process was AlSi10Mg gas atomized powder with spherical particles of an average diameter between 45 and 75 µm. The aluminum alloy consists of 9.9% silicon and 0.39% magnesium. The machine features a closed-loop powder handling system including completely inertized hoses for powder transportation, inertized sieving station, and inertized silo for storage. Unused powder during the recoating in the process as well as the unused powder after the process are constantly recycled and regularly refreshed with new powder.

In pre-production, the cylinder head was virtually placed in the build envelope of the machine and a build direction was chosen regarding geometry, estimated process time, and need for support structures. While designing the still necessary support structures, the focus was on preventing deformation and warpage of the part during the process. Another important topic was the later removal of the support structures and the time to print them. To prevent warpage, all areas below a building angle of 45° were supported by block supports. Additionally, cone supports were added for smaller critical points and areas like overhangs or bridges. Cone supports were used as well for thermal dissipation. Internal cavities especially the oil and cooling channels were kept free of support structures. Larger internal cavities, which were accessible for support removal, were built with a reduced amount of block supports compared to outer surfaces.

Before the LPBF process started, the build platform was heated up to 200°C to reduce thermal stress during the printing [50, 51]. The nitrogen atmosphere with 0.01%–0.03% residual oxygen had a flow rate of 200 m^3/h. Laser power for the hatch was 950 W with a scanning speed of 2450 mm/s. For a good balance between productivity and geometrical accuracy, the layer thickness was set to 60 µm. The theoretical build rate of the hatch parameter was 95 cm^3/h per laser. The build job of one cylinder head lasted for roughly 4 days.

After the removal of powder and support structures, all external surfaces of the cylinder head were manually ground and shot blasted with white corundum. To increase material ductility compared to the as-built state, a T6 heat treatment was performed. The temperature for solution annealing was 530°C held for 6 h followed by a quenching in 20°C water and an aging at 200°C for 3 h. After the heat treatment, the cylinder head was shot blasted with white corundum again for a clean and smooth surface appearance. The surface roughness in coolant and oil channels was reduced by a chemical–electrochemical process. In the last step, the cylinder head was machined to the final part geometry, and valve guides, seat rings, valves, and valve springs were assembled (Figure 18).

Component Validation

Test Methodology, Setup, Boundary Conditions

In operation, the cylinder heads undergo complex high dynamic and thermal stresses, where the dynamic share is mainly caused by the internal combustion and thermal share results from temperature pulses spread with an uneven distribution. The valve train forces are insignificant as its influence on the durability is negligible. The resulting

FIGURE 18 Cylinder head in different stages of the manufacturing process; pre-processed (1), manufactured and depowdered (2), support structures removed (3), machined and assembled (4).

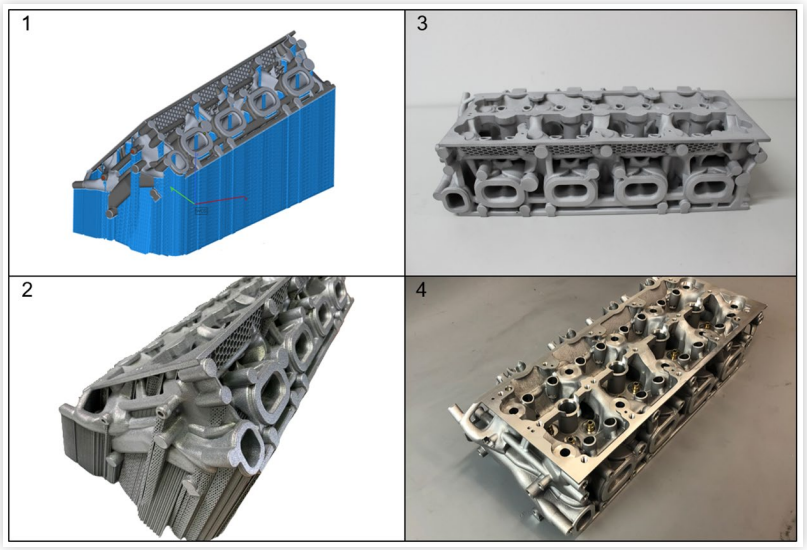

alternating stresses with almost constant temperatures during steady-state operation represent "high-cycle" stresses. Coinciding with external vibrational forces they shift mean stresses and influence the tolerable stress amplitudes of high frequency.

The complexity of the dynamic stresses is a challenge for the selection of a simple, yet representative test method of respective engine components. At DEUTZ AG, an in-house-built hydro-pulse test bench was made available (Figure 19). To replicate the real-time operation, the ignition gas pressure is generated by an oil-hydraulic system up to 550 bar, and the firing order is set according to individual engines. The frequency of the hydraulic pulse in the combustion chamber can be aligned with the engine rpm. A cooling system is integrated to keep the system temperature stable between 50°C and 70°C.

The pressure curve and peak pressure in each combustion chamber are measured and monitored individually. Sensors are positioned next to the combustion chamber to minimize measurement distortions, caused by dynamic effects in hoses and ducts. The test bench is fitted with monitoring devices that automatically shut down the operation as soon as specimen pressure decreases. Plotting ignition pressure against the number

FIGURE 19 The specimen on a test bench.

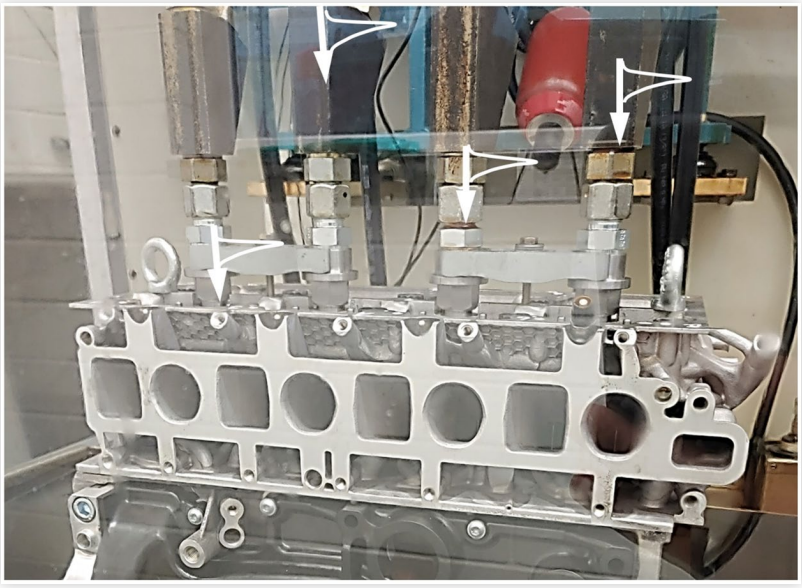

of cycles results in S/N diagram yielding the approximate service limits for the component.

Testing, Results

The AM cylinder head is assembled with original parts such as valve seat inserts, valves, and so forth, and screwed onto a crankcase with an intermediate gasket and original cylinder head bolts. The bolts were fastened according to the tightening instructions of the reference engine. A loss of preload during the first hours of engine operation through thermal expansions was imitated by heating the assembled engine to 120°C. Then, after cooling down a second control of the preload on the screws was conducted, and 18% reduction has been observed, which is in accordance with the experiences of conventional engines with multilayer gaskets. Nevertheless, the test has been performed without settling effects to consider worst-case situation.

The test was started with nominal maximum ignition pressure of 150 bar first. On this level, the AM cylinder head was assumed to be durable at a 100% survival rate. Hence, after 14 million load cycles without any abnormalities, maximum cylinder pressure was increased to 200 bar, where a failure occurred after approximately 9 million cycles. With the component failure, further performance information was achieved and subsequently, the CAE could be verified by means of fractography (Figure 20).

The S/N curve assumptions are evaluated in accordance with the FKM guideline [53], where for aluminum alloys knee points N_D of 10^6 and $N_{D,II}$ of 10^8, and slopes K_I of 5 and K_{II} of 15 are reported. With these frame parameters, a 50% survival probability fatigue strength is determined to be at 170 bar based on the single prototype.

FIGURE 20 S/N curve of the cylinder head for a 50% survival rate, with knee points and slopes [52].

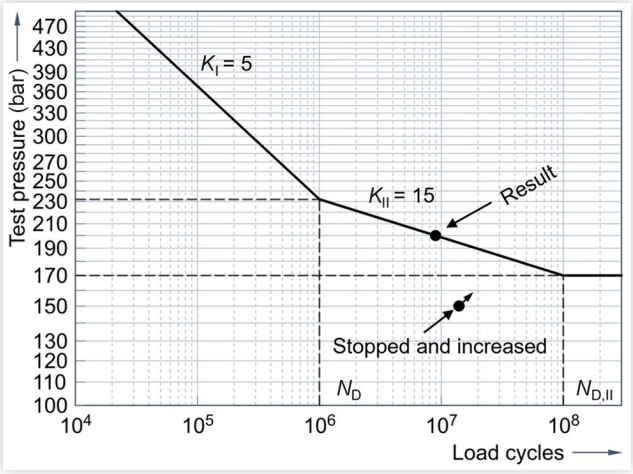

Failure Analysis

On inspection after testing, surface cracks were visible on the oil channel surface of cylinder 3 and cylinder 2 (marked in Figure 21), whereas at cylinder 2 the crack did not propagate.

By cutting the cylinder head at cylinder 3, the fracture propagation became accessible and the crack surface could be analyzed in microscopic detail. The main crack emanated from position 3, as shown in Figure 22. An evidence of surface pores was detected at the area of crack propagation, which weakened the 1.5 mm-thin wall of the oil channel (Figure 23). From here the main crack spread in both directions toward positions 1 and 5, finally splitting the structure at position 1 and 2 completely. Subsequently, secondary cracks were formed at positions 4, 6, and 7, with the main crack ending at position 8 (see Figure 22).

Proceeding the failure analysis, cylinders 1, 2, and 4 were inspected, focusing on the same areas, on regions indicated to be critical by simulation, and on structural defects. In all locations of focus secondary cracks were detected. All cylinders exhibit a similar pore density on their surfaces with slight variations in pore size. The presence of pores not only reduces the cross-section but also concentrates higher stresses, which further infer reduced fatigue strength of the AM cylinder head.

Simulation and Testing Correlation

A HCF analysis with the same boundary conditions as used for the hydro-pulse test has been performed to

FIGURE 21 Cylinder head after fatigue testing; crack areas at cylinder 2 (bottom left) and at cylinder 3 (bottom right).

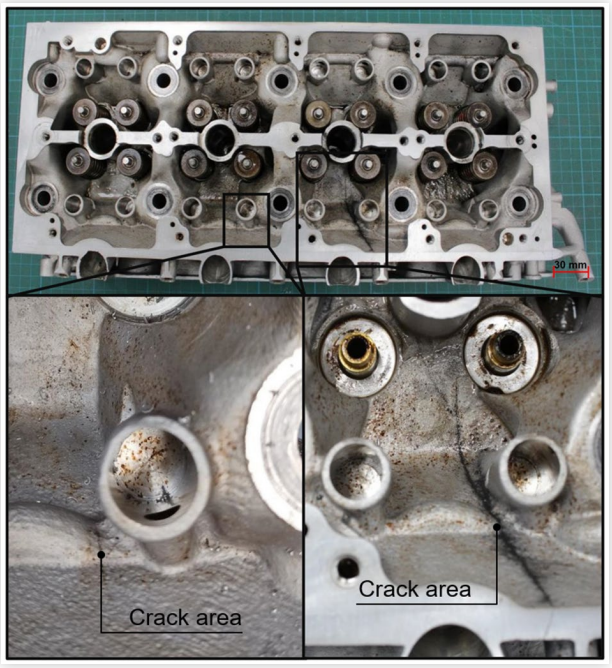

FIGURE 22 Crack propagation.

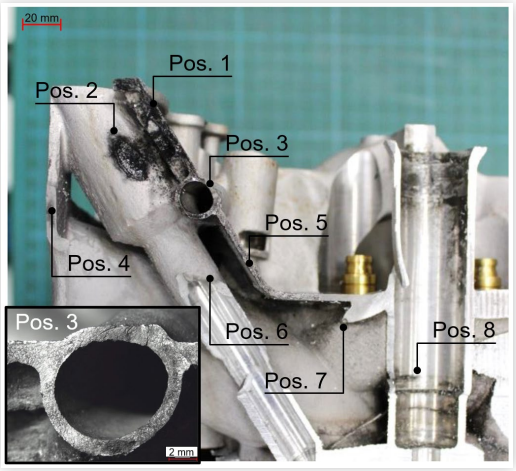

validate the simulation methodology and defined LPBF material properties:

- Structure at room temperature
- Cyl. pressure during fracture (200 bar)
- Measured cyl. head bolt pretension forces

In Figure 24 minimum safety factors in the crack area of cylinders 2 and 3 for R = const. and σ_m = const. are shown. On the connection radii of the HLA housings to the pressurized oil channels, relatively low safety factors have been observed. In both areas safety factors for R = const. show very similar values. On the other hand, the minimum safety factor for σ_m = const. is lower than at cylinder 2, considering that the crack has been propagating at cylinder 3 and led to the ending of the test. Nevertheless, results show that fatigue safety factors are well above the defined design criteria.

A further example of the correlation between simulation and measurement is shown in Figure 25 for another

FIGURE 23 Surface topography with pore accumulation near the crack (Pos. 3).

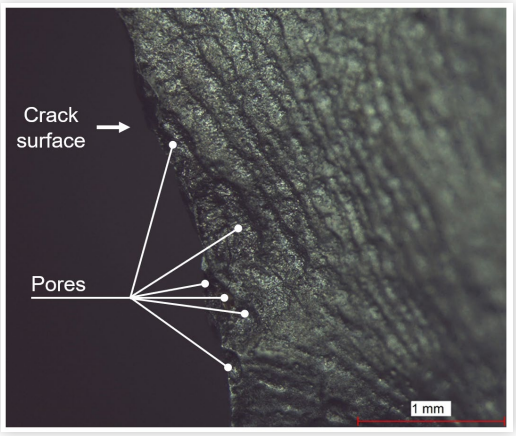

FIGURE 24 Simulation and testing correlation at the crack area between the HLA housings and pressurized oil channels of cylinders 2 and 3.

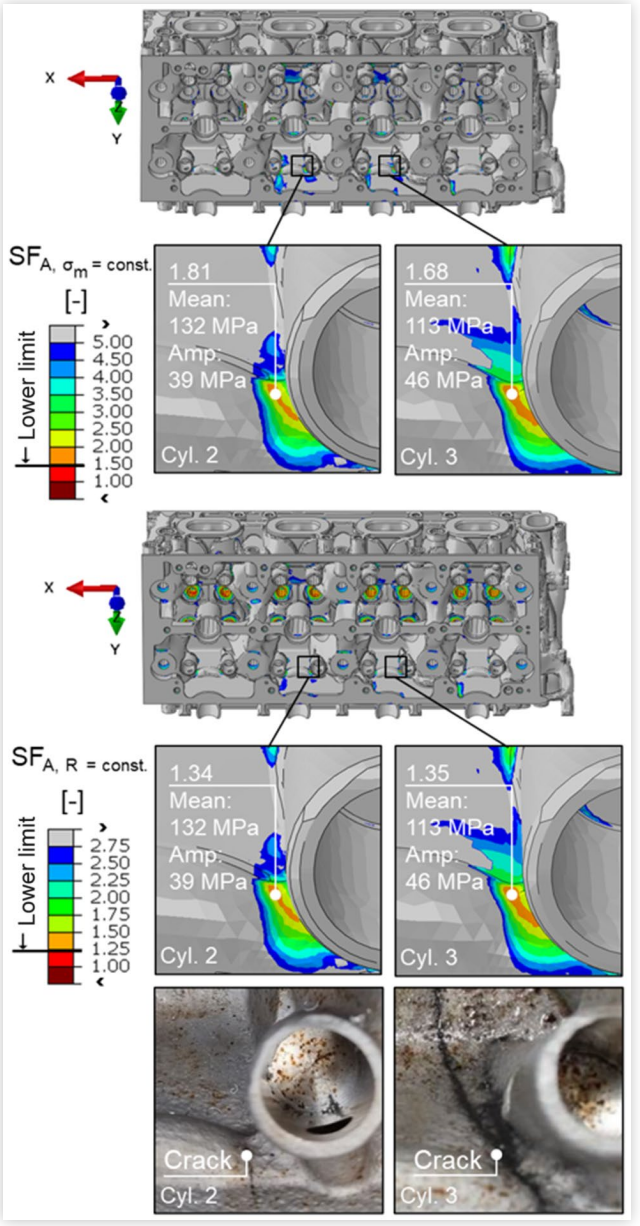

local area between the cylinders, where relatively low safety factors due to high dynamic stress amplitudes have been observed.

Through correlating simulation and testing, predictive performance of the simulation methodology regarding relatively weaker areas have been confirmed. Material analysis suggested that consideration of an additional safety margin during the evaluation of fatigue safety factors for LPBF components may be useful. In addition, in the next section further optimization potentials from the process and material point of view have been discussed.

FIGURE 25 Simulation and testing correlation at the area between the cylinders.

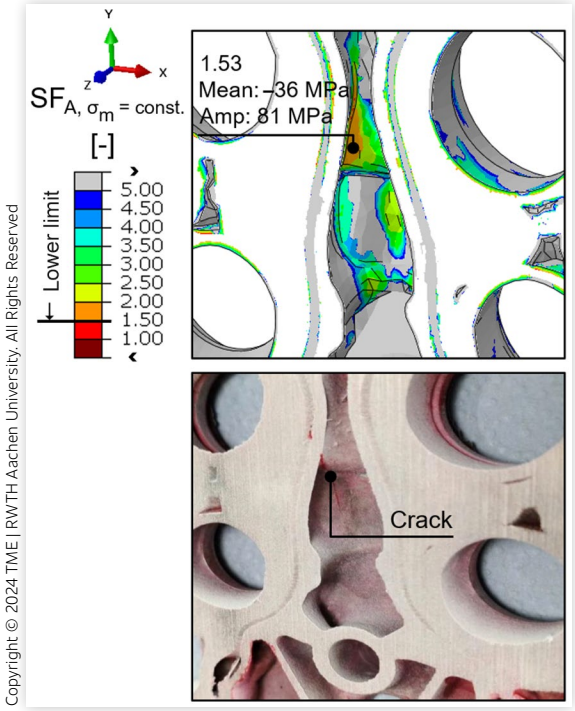

Further Optimization Potentials under Conflicting Goals

Material Usage

The cylinder head in this project was designed exploiting the design freedom of AM to reduce weight. Together with the arterial cooling concept and oil channels this led to a complex geometry even for AM. To reduce the latter, support structures for the lightweight cylinder head, a build direction, and an overhang constraint were chosen during the TO as a basis for designing AM methods applied during the design of the cylinder head. In pre-production of the cylinder head the focus during designing the still necessary support structures was on preventing deformation and warpage of the part during the manufacturing process. Another important topic was the removal of the support structures after completing the manufacturing process, e.g., internal cavities and oil or cooling channels had to be free of supports. Additionally, the time needed to produce the support structures had to be considered as well. The volume of the cylinder head was 3505 cm^3 and the volume of the support structure was 1194 cm^3, making it 34% of the parts volume. This is not unusual for AM. Depending on the complexity of a part, the volume of the support structures can even exceed the volume of the part. But still, the volume of the support structures should be reduced, because support structures increase the cost of the manufactured part in three ways: They increase process time, powder consumption, and post-process time, e.g., support removal and surface grinding. This is of minor importance for prototyping in a one-piece flow but must be considered for series production. Avoiding low build angles, large overhangs, and wide bridges would result in a minimized amount of support structures, which on the other hand may deteriorate the mechanical performance of the cylinder head under a given weight target. Hence, alternative build directions should be analyzed to reduce support structure usage while maintaining the component robustness.

Powder Composition and Post-Treatment

AlSi10Mg is by far the most researched and produced aluminum alloy in AM. The powder is easily accessible by machine suppliers or powder manufacturers.

Material properties of AlSi10Mg in as-built condition depend on various factors such as powder quality and printing parameters, which are together with the optimization of T6 heat treatment parameters under extensive research to achieve the best possible final mechanical properties. While the quasi-static strength values, tensile, and yield strength of additively manufactured AlSi10Mg exceed those of cast material in as-built condition, the same cannot be said for ductility and the fatigue properties. The cylinder head was T6 heat treated to achieve better ductility, which resulted in altering the fine microstructure of the as-built material and lower ultimate and yield strength. Previous studies showed that with optimal layout of heat treatment parameters strength values of the cast materials can be reached [54, 55, 56, 57, 58].

Improvement of the structural strength of the cylinder head at elevated temperatures could be possible with the use of AlSi10Mg(Cu), a copper-alloyed version of the AlSi10Mg material [59, 60] or particle-reinforced AlSi10Mg versions [61, 62]. But even a completely new aluminum alloy especially developed for AM should be considered since AlSi10Mg was originally developed for casting. The newly researched aluminum alloys are promising regarding tensile strength and elongation, but fatigue resistance and thermal conductivity must be investigated as well [63, 64, 65, 66, 67].

Together with the optimization of the heat treatment parameters, even build platform temperatures should be considered in the future [50, 51, 68].

Manufacturing Parameters

In addition to microstructure and inherent defects, mechanical properties are also density-related [69]. The LPBF build parameter in this study features high-power

laser with 950 W power and, therefore, made for high-volume production with a theoretical build rate of 95 cm^3/h per laser. To achieve this build rate the volumetric energy density (VED) [70] was kept low and a density of >99% was accepted. Higher densities are possible with higher VEDs, but since the laser power is almost at the maximum level of the machine, the only options are to reduce scanning speed, layer thickness, or hatch spacing, which inevitably results in lower build rates [71, 72]. Instead of altering the process parameters, a possible further improvement of the cylinder head could be a hot isostatic pressing to achieve higher density [70, 73, 74].

Design Optimization

After defining the concept design of the cylinder head, the geometry of relatively critical areas and the build direction on the plate can be optimized in order to achieve better surface qualities and avoid downfacing surfaces [41]. Additionally, component strength can be improved even further by reducing the possible buildup of residual stresses and avoiding stress concentrations during the LPBF process with proper design.

Summary and Conclusions

Due to its impact on fuel consumption, exhaust gas emissions, and vehicle dynamics, there is continuous demand for weight reduction of the vehicle components. As one of the heaviest systems of a vehicle, the weight reduction potential of powertrain components has been widely analyzed.

Exploiting the design freedom brought by AM, in the scope of this work a passenger car cylinder head with a borderline lightweight design concept has been introduced. It was demonstrated that in comparison with current casting technology 30% weight reduction can be achieved under series development criteria by using automated TO tools.

Thermomechanical HCF performance of the prototype design has been validated in CAE under worst-case engine operation conditions, using the measured quasi-static and alternating strength values of the LPBF material from test samples. Additionally, the effect of AA duration on material properties during T6 heat treatment has been investigated. It has been observed that shortening AA from 12 to 3 h resulted in higher average ultimate strength at elevated temperatures.

A prototype cylinder head has been manufactured with LPBF process using AlSi10Mg powder, and the component durability has been validated using a hydropulse test with the maximum cylinder pressure of the reference Diesel engine, 150 bar. A target of 10 million load cycles has been achieved and proceeded until 14 million load cycles without any visible failure of the component.

In order to identify the durability limit and analyze the failure mechanism of the cylinder head, cylinder pressure has been further increased to 200 bar. Based on the findings a maximum allowable cylinder pressure of 170 bar for HCF load has been calculated according to FKM guidelines, which is significantly over the maximum cylinder pressure of the reference Diesel engine. Simulation methodology and used material properties have been validated by means of a simulation and measurement comparison, where relatively low safety factors have been observed at the crack areas. A fractography analysis has been performed to evaluate the material microstructure at the crack areas. Various pores with irregular distribution have been observed, having relatively larger diameters than at the surface of a conventional cast material. Hence, consideration of an additional safety margin during the CAE validation of LPBF component has been suggested.

Finally, the effect of material, heat treatment, and process parameters on mechanical performance have been discussed for further increase of fatigue durability at higher cylinder pressures. Under the trade-off between manufacturing costs, times, and mechanical performance, optimization of the used aluminum alloy and post-treatment parameters offer a commercially good potential with regard to further optimization for future series applications.

Future hybrid powertrains with range extender applications offer further weight reduction potential for base engine components, since internal combustion engines are mostly operated under partial load conditions subjected to lower thermomechanical loads.

Acknowledgements

This work was supported by the Federal Ministry for Economic Affairs and Climate Action of Germany (BMWK). The authors would like to thank Fraunhofer ILT for performing the tensile and fatigue tests.

Contact Information

Can Kayacan, corresponding author
Chair of Thermodynamics of Mobile Energy Conversion Systems of RWTH Aachen University
kayacan_c@tme.rwth-aachen.de

References

1. Bader, B. et al, “Multi Material Design. A Current Overview of the Used Potential in Automotive Industries”, Technologies for economical and functional lightweight design: Conference proceedings 2018, Springer Vieweg, Berlin, Heidelberg.

2. Bax & Company, "A Vision on the Future of European Lightweighting," 2020.
3. Rosenthal, S. et al., "Lightweight in Automotive Components by Forming Technology," *Automotive Innovation* 3, no. 3 (2020): 195-209.
4. Taub, A.I. and Luo, A.A., "Advanced Lightweight Materials and Manufacturing Processes for Automotive Applications," *MRS Bulletin* 40, no. 12 (2015): 1045-1054.
5. Singh, S. et al., "An Overview of Vehicular Emission Standards," *Mapan* 38, no. 1 (2022): 241-263.
6. Tietge, U. et al., "CO_2 Emissions from New Passenger Cars in Europe: Car Manufacturers' Performance in 2021," International Council on Clean Transportation, Washington, DC, 2022.
7. Bui, A. and Yang, Z., "U.S. Light-Duty Vehicle Greenhouse Gas Standards for Model Years 2023–2026 and Corporate Average Fuel Economy Standards for Model Years 2024–2026," International Council on Clean Transportation, Washington, DC, 2022.
8. "Japan 2030 Fuel Economy Standards," International Council on Clean Transportation, Washington, DC, 2019.
9. International Energy Agency, "CO_2 Emissions in 2022," 2023.
10. Helms, H. and Kraeck, J., "Energy Savings by Light-Weighting—2016 Update," Institut für Energie- und Umweltforschung Heidelberg, 2016.
11. Tang, G. et al., "Study on Pollutant Emission Characteristics of Different Types of Diesel Vehicles during Actual Road Cold Start," *Science of the Total Environment* 823 (2022): 153598.
12. Roberts, A. et al., "Internal Combustion Engine Cold-Start Efficiency: A Review of the Problem, Causes and Potential Solutions," *Energy Conversion and Management* 82 (2014): 327-350.
13. Lutsey, N., "Review of Technical Literature and Trends Related to Automobile Mass-Reduction Technology," Institute of Transportation Studies, California, 2010.
14. Raedt, H.W. et al., "Lightweight Forging Initiative—Phase II: Lightweight Design Potential for a Light Commercial Vehicle," *ATZ Worldwide* 118, no. 3 (2015): 48-53.
15. Patil, C. et al., "A Review of Engine Downsizing and Its Effects," *International Journal of Current Engineering and Technology* 7, no. 7 (2017): 319-324.
16. Kumke, M. et al., "Methods and Tools for Identifying and Leveraging Additive Manufacturing Design Potentials," *International Journal on Interactive Design and Manufacturing (IJIDeM)* 12, no. 2 (2017): 481-493.
17. Gralow, M. et al., "Biomimetic Design and Laser Additive Manufacturing—A Perfect Symbiosis?" *Journal of Laser Applications* 32, no. 2 (2020).
18. Jihong, Z.H.U. et al., "A Review of Topology Optimization for Additive Manufacturing: Status and Challenges," *Chinese Journal of Aeronautics* 34, no. 1 (2021): 91-110.
19. Barbieri, S.G. et al., "A Design Strategy Based on Topology Optimization Techniques for an Additive Manufactured High Performance Engine Piston," *Procedia Manufacturing* 11 (2017): 641-649.
20. MAHLE, "MAHLE Produces High-Performance Aluminum Pistons Using 3D Printing for the First Time," Press Release, 2020.
21. Bassoli, E. et al., "Design for Additive Manufacturing and for Machining in the Automotive Field," *Applied Sciences* 11, no. 16 (2021): 7559.
22. Marchesi, T.R. et al., "Topologically Optimized Diesel Engine Support Manufactured with Additive Manufacturing," *IFAC-PapersOnLine* 48, no. 3 (2015): 2333-2338.
23. Chiandussi, G. et al., "Topology Optimisation of an Automotive Component without Final Volume Constraint Specification," *Advances in Engineering Software* 35, no. 10-11 (2004): 609-617.
24. Cavazzuti, M. et al., "High Performance Automotive Chassis Design: A Topology Optimization Based Approach," *Structural and Multidisciplinary Optimization* 44, no. 1 (2010): 45-56.
25. Chao, L. et al., "Conceptual and Detailed Design of an Automotive Engine Cradle by Using Topology, Shape, and Size Optimization," *Structural and Multidisciplinary Optimization* 51, no. 2 (2014): 547-564.
26. Chao, L. and Yong, I.K., "Topology, Size and Shape Optimization of an Automotive Cross Car Beam," *Proceedings of the Institution of Mechanical Engineers, Part D: Journal of Automobile Engineering* 229, no. 10 (2014): 1361-1378.
27. Lindemann, B. et al., "Additive Manufacturing in Modern Combustion Engines," *MTZ Worldwide* 81 (2020): 40-45.
28. Bey, R. et al., "Weight Reduction and Functional Improvement of Future Combustion Engines with Additive Manufacturing and Composite Materials," in *30th Aachen Colloquium Sustainable Mobility*, Aachen, Germany, 2021.
29. Kayacan, C., Zabirov, A. et al., "LeiMot—Lightweight Engine Helps Reducing CO_2 Emissions," *Transportation Research Procedia* 72 (2023): 1021-1028.
30. Eschenauer, N. et al., *Applied Structural Mechanics* (Berlin, Heidelberg: Springer, 1997)
31. Christensen, P.W. and Klarbring, A., *An Introduction to Structural Optimization* (Dordrecht: Springer Science + Business Media B.V., 2009)
32. Choi, W.H. et al., "Comparison Study of Some Commercial Structural Optimization Software Systems," *Structural and Multidisciplinary Optimization* 54, no. 3 (2016): 685-699.
33. Bendsøe, M.P., "Optimal Shape Design as a Material Distribution Problem," *Structural Optimization* 1 (1989): 193-202.
34. Tyflopoulos, E. and Steinert, M., "A Comparative Study of the Application of Different Commercial Software for Topology Optimization," *Applied Sciences* 12, no. 2 (2022): 611.

35. Niu, F. et al., "A General Formulation of Structural Topology Optimization for Maximizing Structural Stiffness," *Structural and Multidisciplinary Optimization* 43, no. 4 (2010): 561-572.
36. Prager, W., *Optimality Criteria in Structural Design* (San Diego, CA: University of California, 1968)
37. Guan, J. and Zhang, W., "Improved Topological Optimization Method Based on Particle Swarm Optimization Algorithm," *IEEE Access* 10 (2022): 52067-52074.
38. Yang, S. et al., "An Adaptive Multi-Step Varying-Domain Topology Optimization Method for Spot Weld Design of Automotive Structures," *Structural and Multidisciplinary Optimization* 59, no. 1 (2018): 291-310.
39. Rodrigues, H. and Fernandes, P., "A Material Based Model for Topology Optimization of Thermoelastic Structures," *International Journal for Numerical Methods in Engineering* 38 (1995): 1951-1965.
40. Jiang, J. et al., "Support Structures for Additive Manufacturing: A Review," *Journal of Manufacturing and Materials Processing* 2, no. 4 (2018): 64.
41. Kranz, J. et al., "Design Guidelines for Laser Additive Manufacturing of Lightweight Structures in TiAl6V4," *Journal of Laser Applications* 27, no. S1 (2014): S14001.
42. Zhou, M. et al., "Checkerboard and Minimum Member Size Control in Topology Optimization," *Structural and Multidisciplinary Optimization* 21 (2001): 152-158.
43. Szasz, C. et al., "Effizienter Einsatz von CAE und Versuch bei der Entwicklung von Motoren für Baumaschinen," *ATZoffhighway* 7, no. 2 (2014): 60-69.
44. Xu, S. et al., "Effect of Heat Treatment on the Anisotropic Mechanical Properties of AlSi10Mg Fabricated by Selective Laser Melting," *Journal of Materials Engineering and Performance* (2023): 1-14.
45. Tan, S. et al., "Anisotropy Reduction of Additively Manufactured AlSi10Mg for Metal Mirrors," *Journal of Materials Science* 57, no. 25 (2022): 11934-11948.
46. Chen, S. et al., "Effect of Heat Treatment on the Anisotropy in Mechanical Properties of Selective Laser Melted AlSi10Mg," *Materials Science and Engineering: A* 858 (2022): 144130.
47. Zhang, A. and Li, Y., "Thermal Conductivity of Aluminum Alloys—A Review," *Materials* 16, no. 8 (2023): 2972.
48. Jeong, C., "High Temperature Mechanical Properties of Al-Si-Mg-(Cu) Alloys for Automotive Cylinder Heads," *Materials Transactions* 54, no. 4 (2013): 588-594.
49. Zhang, B. et al., "Defect Formation Mechanisms in Selective Laser Melting: A Review," *Chinese Journal of Mechanical Engineering* 30, no. 3 (2017): 515-527.
50. Amir, B. et al., "Experimental Investigation on the Effect of Platform Heating on the Dynamic Mechanical Properties of Selective Laser Manufacturing of AlSi10Mg Alloy," *EPJ Web of Conferences* 250 (2021): 05016.
51. Wang, L. et al., "Investigation of Performance and Residual Stress Generation of AlSi10Mg Processed by Selective Laser Melting," *Advances in Materials Science and Engineering* 2018 (2018): 1-12.
52. At DEUTZ AG all measuring devices are calibrated in regular interval and are monitored continuously. In accordance with DIN 1319, the measured ignition pressure in the cylinder has an accuracy error less than 1%. Since in this project's framework only one sample was tested, the results could be interpreted with S/N-curve for only 50% probability of endurance limit, which can be considered as the mean value in this case. From the experience from past results, the mean value has the accuracy of ±4.4%, in an assumed logarithmic scattering range of T = 1/1.3.
53. Forschungskuratorium Maschinenbau (FKM), "FKM-Richtlinie—Rechnerischer Festigkeitsnachweis für Maschinenbauteile aus Stahl," Eisenguss und Aluminiumwerkstoffen, 2020.
54. Hitzler, L. et al., "Heat Treatments and Critical Quenching Rates in Additively Manufactured Al–Si–Mg Alloys," *Materials* 13, no. 3 (2020): 720.
55. Kempen, K. et al., "Mechanical Properties of AlSi10Mg Produced by Selective Laser Melting," *Physics Procedia* 39 (2012): 439-446.
56. Iturrioz, A. et al., "Selective Laser Melting of AlSi10Mg Alloy: Influence of Heat Treatment Condition on Mechanical Properties and Microstructure," *Welding in the World* 62, no. 4 (2018): 885-892.
57. Aboulkhair, N.T. et al., "On the Precipitation Hardening of Selective Laser Melted AlSi10Mg," *Metallurgical and Materials Transactions A* 46, no. 8 (2015): 3337-3341.
58. Qian, Y. et al., "Comparative Study of Performance Comparison of AlSi10Mg Alloy Prepared by Selective Laser Melting and Casting," *Journal of Materials Science & Technology* 41 (2020): 199-208.
59. Cai, C. et al., "Microstructure Evolution of AlSi10Mg(Cu) Alloy Related to Isothermal Exposure," *Materials* 11, no. 5 (2018): 809.
60. Garmendia, X. et al., "Microstructure and Mechanical Properties of Cu-Modified AlSi10Mg Fabricated by Laser-Powder Bed Fusion," *Materialia* 9 (2020): 100590.
61. Wang, Y. et al., "Investigation of Porosity and Mechanical Properties of Graphene Nanoplatelets-Reinforced AlSi10 Mg by Selective Laser Melting," *Journal of Micro and Nano-Manufacturing* 6, no. 1 (2017): 010902.
62. Xiao, Y.K. et al., "Effect of Nano-TiB2 Particles on the Anisotropy in an AlSi10Mg Alloy Processed by Selective Laser Melting," *Journal of Alloys and Compounds* 798 (2019): 644-655.
63. Agrawal, P. et al., "Additively Manufactured Novel Al-Cu-Sc-Zr Alloy: Microstructure and Mechanical Properties," *Additive Manufacturing* 37 (2021): 101623.

64. Babu, A.P. et al., "Laser Powder Bed Fusion of High Solute Al-Zn-Mg Alloys: Processing, Characterisation and Properties," *Materials & Design* 196 (2020): 109183.
65. Belelli, F. et al., "Development of a Novel High-Temperature Al Alloy for Laser Powder Bed Fusion," *Metals* 11, no. 1 (2020): 35.
66. Deillon, L. et al., "A New High Strength Al–Mg–Sc Alloy for Laser Powder Bed Fusion with Calcium Addition to Effectively Prevent Magnesium Evaporation," *Journal of Materials Processing Technology* 300 (2022): 117416.
67. Knoop, D. et al., "A Tailored AlSiMg Alloy for Laser Powder Bed Fusion," *Metals* 10, no. 4 (2020): 514.
68. Casati, R. et al., "Effects of Platform Pre-Heating and Thermal-Treatment Strategies on Properties of AlSi10Mg Alloy Processed by Selective Laser Melting," *Metals* 8, no. 11 (2018): 954.
69. Kan, W.H. et al., "A Critical Review on the Effects of Process-Induced Porosity on the Mechanical Properties of Alloys Fabricated by Laser Powder Bed Fusion," *Journal of Materials Science* 57, no. 21 (2022): 9818-9865.
70. Giovagnoli, M. et al., "Effect of Different Heat-Treatment Routes on the Impact Properties of an Additively Manufactured AlSi10Mg Alloy," *Materials Science and Engineering: A* 802 (2021): 140671.
71. Buchbinder, D. et al., "High Power Selective Laser Melting (HP SLM) of Aluminum Parts," *Physics Procedia* 12 (2011): 271-278.
72. Aboulkhair, N.T. et al., "Reducing Porosity in AlSi10Mg Parts Processed by Selective Laser Melting," *Additive Manufacturing* 1, no. 4 (2014): 77-86.
73. Hafenstein, S. et al., "Hot Isostatic Pressing of Aluminum–Silicon Alloys Fabricated by Laser Powder-Bed Fusion," *Technologies* 8, no. 3 (2020): 48.
74. Schneller, W. et al., "Effect of HIP Treatment on Microstructure and Fatigue Strength of Selectively Laser Melted AlSi10Mg," *Journal of Manufacturing and Materials Processing* 3, no. 1 (2019): 16.